Determination of the Absolute Photoionization Cross Sections of CH3 and I Produced from a Pyrolysis Source, by Combined Synchrotron and Vacuum Ultraviolet Laser Studies†

ARTICLE *in* THE JOURNAL OF PHYSICAL CHEMISTRY A · NOVEMBER 2009

Impact Factor: 2.69 · DOI: 10.1021/jp909414d

Determination of the Absolute Photoionization Cross Sections of CH_3 and I Produced from a Pyrolysis Source, by Combined Synchrotron and Vacuum Ultraviolet Laser Studies†

Bérenger Gans, Luiz A. Vieira Mendes,§ Séverine Boyé-Péronne, Stéphane Douin, Gustavo Garcia,|| Héloïse Soldi-Lose,|| Barbara K. Cunha de Miranda,§,⊥ Christian Alcaraz,⊥ Nathalie Carrasco,# Pascal Pernot,⊥ and Dolores Gauyacq*

Laboratoire de Photophysique Moléculaire, CNRS UPR 3361, Univ. Paris-Sud 11, Bât. 210, F-91405 Orsay Cédex, France

Received: September 30, 2009; Revised Manuscript Received: November 5, 2009

A pyrolysis source coupled to a supersonic expansion has been used to produce the CH_3 radical from two precursors, iodomethane CH_3I and nitromethane CH_3NO_2. The relative ionization yield of CH_3 has been recorded at the SOLEIL Synchrotron Radiation source in the range 9.0−11.6 eV, and its ionization threshold has been modeled by taking into account the vibrational and rotational temperature of the radical in the molecular beam. The relative photoionization yield has been normalized to an absolute cross section scale at a fixed wavelength (118.2 nm, $\sigma_i^{CH_3} = 6.7^{+2.4}_{-1.8}$ Mb, 95% confidence interval) in an independent laboratory experiment using the same pyrolysis source, a vacuum ultraviolet (VUV) laser, and a carefully calibrated detection chain. The resulting absolute cross section curve is in good agreement with the recently published measurements by Taatjes et al.,[1] although with an improved signal-to-noise ratio. The absolute photoionization cross section of CH_3I at 118.2 nm has also been measured to be $\sigma_i^{CH_3I} = (48.2 \pm 7.9)$ Mb, in good agreement with previous electron impact measurements. Finally, the photoionization yield of the iodine atom in its ground state $^2P_{3/2}$ has been recorded using the synchrotron source and calibrated for the first time on an absolute cross section scale from our fixed 118.2 nm laser measurement, $\sigma_i^{I^2P_{3/2}} = 74^{+33}_{-23}$ Mb (95% confidence interval). The ionization curve of atomic iodine is in good agreement, although with slight variations, with the earlier relative ionization yield measured by Berkowitz et al.[2] and is also compared to an earlier calculation of the iodine cross section by Robicheaux and Greene.[3] It is demonstrated that, in the range of pyrolysis temperature used in this work, all the ionization cross sections are temperature-independent. Systematic care has been taken to include all uncertainty sources contributing to the final confidence intervals for the reported results.

I. Introduction

Hydrocarbon radicals play an important role in planetary atmospheres, particularly in Titan, the largest moon of Saturn, which presents a dense atmosphere mainly composed of dinitrogen N_2 with a large amount of methane CH_4 (around 1.5% in the stratosphere). Among all the gas-phase reactions in the upper atmosphere of Titan, photodissociation plays an important role inducing formation and destruction of many species by the solar radiation.[4] In particular, the photolysis of CH_4 by solar photons around 121.6 nm (solar Lyman-α) gives rise to the formation of small hydrocarbon radicals, while N_2 is dissociated by vacuum ultraviolet (VUV) radiation and by high-energy electrons from Saturn's magnetosphere. The resulting small radicals further recombine or undergo a chain of reactions leading to the production of numerous large hydrocarbons and nitriles, especially unsaturated polyynes and cyanopolyynes.

Branching ratios of the methane photolysis products, i.e., the CH_3, CH_2, and CH radicals, should be determined with the highest possible degree of accuracy to be included in the photochemical models of Titan's atmosphere. Hébrard et al.[5] evaluated the effect of accurately studying the reactions of interest for Titan at low temperature. One important result of this paper is the identification of a short list of seven key reactions controlling the uncertainty on the present photochemical model for Titan's atmosphere. In this list, the photolysis of methane appears as one of the most influential processes in the whole stratosphere and upper atmosphere.

However, an evaluation of the existing literature[6] on CH_4 photolysis pathways at Lyman-α highlighted contradictory values on the branching ratios. Many laboratory experiments aiming at these branching ratio measurements involve mass analysis of the photofragments through VUV photoionization of these radicals. Nevertheless, to convert such mass spectrometry investigations into quantified branching ratios, absolute photoionization cross sections of all radicals under consideration are needed with a good accuracy. Absolute photoionization cross sections of several stable hydrocarbons have been measured earlier (see for instance refs 7–11). However, absolute photoionization cross sections of radicals are far less well-known.[12–14] One challenging issue is to produce these radicals with sufficient quantities and in a well-controlled way, to avoid chemical recombination or reactivity, that means in the diluted gas phase. The other difficulty is to determine their absolute concentration. With the aim of characterizing them, two kinds of radical

† Part of the "Benoît Soep Festschrift".

* Author to whom correspondence should be addressed. E-mail: dolores.gauyacq@u-psud.fr.

§ Laboratorio de Espectroscopia e Laser, Universidade Federal Fluminense, Niteroi, Brazil.

|| Synchrotron SOLEIL, L'Orme des Merisiers, St Aubin, France.

⊥ Laboratoire de Chimie-Physique, CNRS UMR 8000, Univ. Paris-Sud 11, France.

Laboratoire ATMOS, Univ. Versailles St Quentin, CNRS, France.

10.1021/jp909414d

sources have been developed in the past, either pyrolysis sources[15–18] or photolysis sources.[11,12,19–21] For each of them, suitable precursors have to be selected to efficiently dissociate into the desired radical.

The absolute photoionization cross section of the methyl radical (CH_3), the second main product of the methane photolysis in the upper atmosphere of Titan according to the critical review of Hebrard et al.,[22] and its relative formation yield in the methane photolysis at 121.6 nm are crucial data for Titan's atmospheric models. Very recently, Taatjes et al.[1] measured the absolute photoionization cross section of CH_3 produced from the photolysis of several precursors by means of two independent methods: (i) by using a pulsed laser-photolysis/time-resolved synchrotron mass spectrometry and (ii) by using photolysis in a molecular-beam ion-imaging apparatus. The synchrotron photoionization measurements have been carried out by using two precursors, acetone and methyl vinyl ketone, for which the photoionization cross sections at given UV wavelengths are known.[23,24] The measurements involving a molecular-beam ion-imaging apparatus have been performed on the 266 nm photolysis of the CH_3I precursor and were extracted by evaluating the iodine atom photoionization cross section from refs 2 and 3.

The present work aims at two goals: (i) the measurement of the absolute photoionization cross section of methyl radical CH_3 and iodine atom $I(^2P_{3/2})$ by using a pyrolysis source and the comparison of our results with those of ref 1; (ii) the careful statistical evaluation of the uncertainties attached to this measurement to fulfill the requirements for implementation in planetary models.[25,26]

The pyrolysis source was chosen in the present study because of its high radical production efficiency and because of the lack of a photolysis laser attached to the beamline at the synchrotron radiation experiment. Moreover, the same pyrolysis source was used in the laboratory VUV laser experiment to work within experimental conditions for the radical production as close as possible to those of the synchrotron-based experiments. Furthermore, this procedure allowed us to complement the data obtained at the synchrotron radiation by the laser-based experimental data and vice versa. Special attention was given to the subsequent reactivity occurring in the source, as detailed in the text below. Finally, a major point of this work was to ensure that the measurement of the CH_3 and I photoionization absolute cross section was not temperature-dependent, in the range of pyrolysis temperatures used in this work.

II. Experimental Section

The present experiments have been carried out with two independent and complementary experimental setups, by using either a synchrotron radiation-based or a laser-based molecular beam-mass spectrometer apparatus. Nevertheless, both apparatuses used duplicated pyrolysis sources, to work with similar conditions of radical production.

A. Pyrolysis Source. The CH_3 radicals are produced from two commercial precursor molecules (methyl iodide CH_3I, Sigma-Aldrich 99.5% or nitromethane CH_3NO_2, Sigma-Aldrich 99%) in a pyrolysis source which has been described elsewhere.[15,16,18] Briefly, a continuous molecular beam is produced in the expansion chamber through a water-cooled nozzle (70 μm diameter in the laser experiment, 50 μm diameter in the synchrotron experiment) from a gas mixture composed by the precursor molecule and rare gas. To limit the reactivity of the pyrolysis products, the precursors are diluted in a large excess of helium or argon upstream to the nozzle (a few percent of CH_3I or CH_3NO_2). The typical backing pressure is about 100−200 mbar in the laser-based experiment and 1 bar in the synchrotron-based experiment. The expanded gas enters a SiC tube (1 mm diameter) heated with an adjustable current applied between two electrodes. These electrodes are separated by approximately 3 mm and fixed close to the end of the tube to minimize bimolecular reactions. A typical heating power of about 10−70 W is applied, corresponding to a temperature range of 800−1450 °C. The temperature is measured by a pyrometer (KELLER disappearing filament pyrometer, PB 06 AF3) with an estimated relative accuracy of 20 °C.

B. VUV Laser Photoionization Measurements. ***B.1. Time-of-Flight Apparatus.*** The apparatus consists of a continuous molecular beam equipped with the pyrolysis source described above and coupled to a fixed VUV laser source at 118.2 nm and a time-of-flight (TOF) mass spectrometer for analysis.

The output gas mixture from the pyrolysis tube enters the expansion chamber with a typical working pressure maintained to 10^{-4} mbar with a 2000 L/s Edwards diffusion pump. The free molecular jet is skimmed (1 mm diameter) before the ionization region where it crosses at a right angle a VUV laser beam.

The VUV laser beam is generated by nonresonant third harmonic generation in a 20 cm long cell filled with about 5 Torr of Xenon, by focusing the 354.7 nm third harmonic of a pulsed Nd^{3+}:YAG laser (BMI, model 502-D.NS, 10 Hz, 30 mJ @ 355 nm) with a fused-silica plano-convex lens ($f = 120$ mm @ 355 nm). The two unfocused beams (UV at 354.7 nm and VUV at 118.2 nm) are recollimated by a MgF_2 lens and spatially separated by a MgF_2 prism to steer only the 118.2 nm VUV beam into the ionization chamber. The spectral width of the fundamental (1.064 μm) YAG laser beam is about 5 cm^{-1}, leading to an estimated spectral width of about 40 cm^{-1} for the 118.2 nm beam. The relative VUV photon flux is measured by using the photoelectric signal generated by irradiating a gold plate.

The ions produced in the interaction zone are extracted with a double acceleration stage, focused by an Einzel lens and collected by a microchannel plate after a 1.2 m flight tube. The typical mass resolution of the TOF spectrometer, $m/\Delta m$, is about 500 for $m = 15$. Mass spectra are recorded by an oscilloscope (LECROY LC584A 1 GHz) in 50 000 channels of 1 ns width. The ion signal is obtained by integration over a 30−100 ns wide time window centered on the mass peak of interest.

Figure 1 displays typical mass spectra at two different pyrolysis temperatures (panel (a) and (b)) for the CH_3I precursor. The corresponding difference spectrum is also plotted in panel (c). The only products observed in this experiment are CH_3, I, and, to a lesser extent, I_2 and HI. This means that under the operating conditions of our pyrolysis source, subsequent reactions could not be completely avoided, and a compromise was found to form significant amounts of the CH_3 radical and to minimize reactivity. These subsequent reactions are taken into account in the data analysis as discussed in section III.A. Note that mass spectra have been recorded within the same pyrolysis conditions at the synchrotron radiation facility up to 15 eV and demonstrated that no other species were produced in a detectable amount.

B.2. Measurement of the Mass Discrimination Factor of the Detection System. To determine absolute photoionization cross sections, the knowledge of the apparatus function as a function of mass is required. Hence, the mass discrimination factors of the TOF mass spectrometer have been carefully

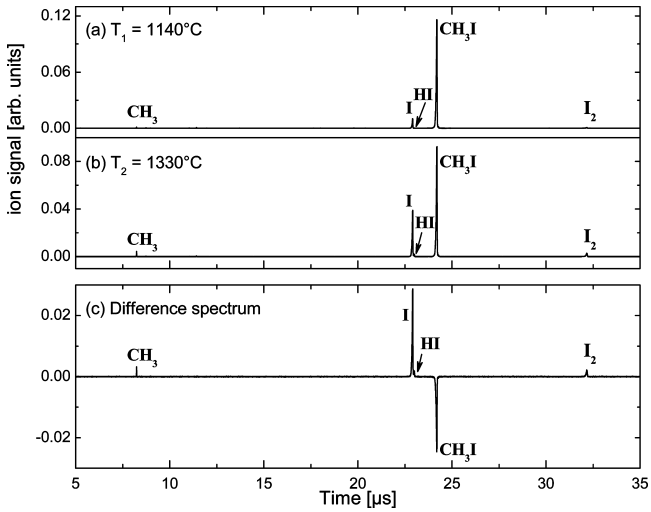

Figure 1. Mass spectra obtained at 118.2 nm from the pyrolysis of CH_3I precursor: (a) $T_1 = 1140$ °C; (b) $T_2 = 1330$ °C; (c) corresponding difference spectrum.

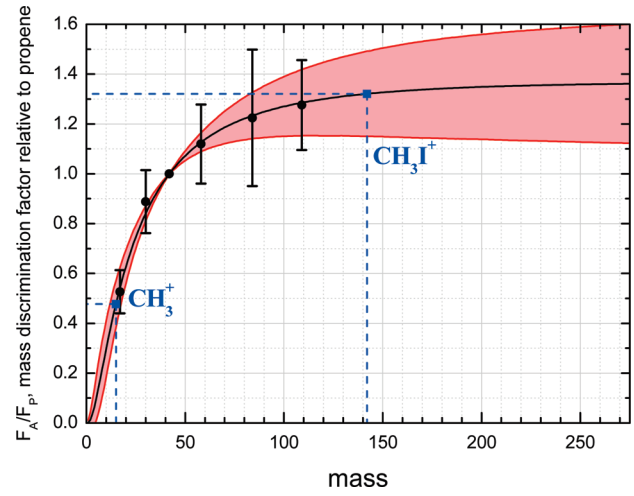

Figure 2. Calibration of the mass discrimination factor of the TOF mass spectrometer used in the laser experiments, with respect to propene. The black dots and error bars represent the experimental values and their 95% confidence intervals. Extrapolation by a sigmoïd model is shown as a black straight line (see the text for details). The red lines represent the sample of model realizations compatible with the experimental data, as obtained by Bayesian data analysis (see text).

measured following the method described by Cool et al.[23] by using six species for which the absolute photoionization cross section value at 118.2 nm is well-known (ammonia, nitrogen monoxide, propene, acetone, cyclohexane, and ethyl bromide). Since propene is a gaseous hydrocarbon with an intermediate mass in the range of the masses used for the apparatus function and since it has a well-known photoionization cross section at 118.2 nm,[9] it has been chosen as a reference for the calibration of the mass apparatus function. For each species, a calibrated mixture of propene P (1−2%) and compound A (1−2%) diluted in helium has been prepared. The ratio of the mass discrimination factors of the species A with respect to propene P has been determined experimentally from the ratio of the corresponding ion signals S_A/S_P

$$\frac{S_A}{S_P} = \frac{P_A}{P_P}\frac{F_A \times \sigma_i^A}{F_P \times \sigma_i^P} \quad (1)$$

where P_A and P_P are the partial pressures in the molecular beam (measured via a Baratron gauge Pfeiffer CMR 361 with an accuracy of 0.2%); σ_i^A and σ_i^P are the absolute photoionization cross sections at 118.2 nm (with $\sigma_i^{NH_3} = 2.0 \pm 0.2$ Mb,[27,28] $\sigma_i^{NO} = 2.0 \pm 0.2$ Mb,[27,29,30] $\sigma_i^{C_3H_6O} = 11.2 \pm 1.1$ Mb,[23] $\sigma_i^{C_6H_{12}} = 21 \pm 4$ Mb,[23] $\sigma_i^{C_2H_5Br} = 18.0 \pm 1.8$ Mb,[10] and $\sigma_i^P = 11.0 \pm 1.1$ Mb[9]); and F_A and F_P are the mass discrimination factors for A and propene, respectively.

The ratio values, F_A/F_P, of the measured mass discrimination factors with respect to that of propene are reported together with their uncertainties in Figure 2. Note that the calibration curve of F_A/F_P must be equal to unity at the mass of propene (mass 42). All the measurements are performed within the same backing pressure conditions in the source chamber (see section II.A above). These apparatus function measurements are recorded at room temperature by using the same source chamber device with the pyrolysis heating system turned off. The knowledge of the mass discrimination factor is a crucial point for the measurement of absolute cross sections. Because for the determination of cross sections in this paper we need to extrapolate the mass discrimination factors, a careful calibration fit with its statistical extrapolation estimate has been performed by using the Bayesian data analysis.

To extrapolate a series of measurements out of the range of a control parameter, we need a model linking the observable to the control parameter and a representation of the measurement uncertainties. From these ingredients, it is possible to get predicted values and the associated confidence interval.

Bayesian data analysis provides a consistent framework for the calibration of a model to a training set and the subsequent probabilistic extrapolation.[31,32] The calibration step estimates the probability density function (pdf) of the model parameters, conditional to the measurements (value and uncertainty) and to the chosen model.

The sigmoïd model, $(F_A/F_P)_{mod}$ (noted below as $(F_{A/P})_{mod}$), is a function of the experimental mass m_{exp} and has three parameters, c_1, c_2, and c_3, as follows

$$(F_{A/P})_{mod}(m_{exp};c_1,c_2,c_3) = \left(0.5 + 0.5\mathrm{erf}\left(\frac{\log\left(\frac{m_{exp}}{c_1}\right)}{c_2}\right)\right) \times c_3$$

Note that this model constrains our calibration curve to pass at $(F_{A/P})_{mod}(0) = 0$, as shown in Figure 2.

The *posterior* pdf of these parameters is

$$p(c_1,c_2,c_3|(F_{A/P})_{exp},(F_{A/P})_{mod}) \propto p((F_{A/P})_{exp}|c_1,c_2,c_3,(F_{A/P})_{mod}) \times p(c_1,c_2,c_3|(F_{A/P})_{mod})$$

where $p(c_1,c_2,c_3|(F_{A/P})_{mod})$ is the *prior* pdf which contains all information on the parameters independent of the measurements. In the present case, one has no prior preference and thus uses

$$p(c_1,c_2,c_3|(F_{A/P})_{mod}) \propto \frac{1}{c_2}$$

which is uniform for c_1 and c_3 and log-uniform for c_2 (a positive scale parameter).

The *likelihood* function $p((F_{A/P})_{exp}|c_1,c_2,c_3,(F_{A/P})_{mod})$ is established from the probabilistic representation of the experimental uncertainties. In the case of normal additive errors, one has

$$p((F_{A/P})_{exp}|c_1,c_2,c_3,(F_{A/P})_{mod}) \propto \exp\left(-\frac{1}{2}\sum_i\left(\frac{(F_{A/P})_{exp\,i} - (F_{A/P})_{mod}(m_{exp\,i};c_1,c_2,c_3)}{u_i((F_{A/P})_{exp})}\right)^2\right)$$

All information about the calibrated parameters can be obtained from their *posterior* pdf. In the present case, these parameters

have no specific interest. The *posterior* pdf is an intermediate to interpolation and extrapolation: the distribution of model values at any point of the curve can be obtained from the *posterior* pdf by the uncertainty propagation formula

$$p((F_{A/P})_{mod}(m')|(F_{A/P})_{exp}, (F_{A/P})_{mod}) =$$

$$\int dc_1 dc_2 dc_3 (F_{A/P})_{mod}(m';c_1, c_2, c_3) \times p(c_1, c_2, c_3|(F_{A/P})_{exp}, (F_{A/P})_{mod})$$

The most convenient way to perform these calculations is by a Monte Carlo approach, using representative samples of the quantities of interest. In a first step, a representative sample of the *posterior* pdf $p(c_1,c_2,c_3|(F_{A/P})_{exp}, (F_{A/P})_{mod})$ is obtained by Markov Chain Monte Carlo. This sample is then used to calculate directly a sample of $(F_{A/P})_{mod}(m')$ values, on which statistical estimates are performed.

The set of data and a sample of model predictions are reported in Figure 2.

B.3. Measurement of the Temperature-Dependent Gas Expansion Function. A second experimental parameter has to be taken into account in these absolute measurements: indeed the temperature of the pyrolysis source can also have an effect on the gas expansion. It leads to a signal decrease with increasing temperature as discussed by Zhang et al.[33] This temperature effect, which induces a variation of the density in the beam, strongly depends on the experimental conditions (backing pressure, pyrolysis source, distance between the skimmer and the pyrolysis tube outlet, skimmer size, ...) but does not depend significantly on masses as noticed by Zhang et al.[33] To determine this effect in terms of an expansion function, the ion signal from nitrogen monoxide (5.5% diluted in helium) has been measured as a function of the temperature within a pertinent range for CH_3I pyrolysis processes, i.e., between 800 and 1400 °C. The NO molecule has been chosen because of its low ionization energy (9.26 eV) and its robustness toward pyrolysis (6.5 eV bond energy).[34] A very small relative linear decrease of the NO^+ signal was observed, following the formula $[-5 \times 10^{-5}T + 1]$, valid for a temperature range between 800 and 1400 °C. This expansion function is shown as a linear fit of the NO^+ signal in Figure 3a. This expansion parameter is accounted for all ion signals observed during the temperature-dependent pyrolysis processes.

C. Synchrotron Photoionization Measurements. The relative photoionization yields were recorded on the DESIRS beamline[35] at the SOLEIL synchrotron facility in St. Aubin (France). This undulator-based beamline[36] delivers tunable radiation in the 5−40 eV energy range. The 6.65 m normal incidence monochromator[35] equipped with a 200 gr/mm grating provides a photon flux of up to 10^{12} ph/s with a resolution of 5 meV at 9 eV for a 100 μm exit slit. To eliminate the higher harmonics photons of the undulator, a gas filter[37] is used and filled with Ar up to 0.30 mbar.

Experiments were performed using the DELICIOUS II spectrometer installed in the differentially pumped vacuum chamber SAPHIRS.[38] This newly developed spectrometer consists of a velocity-map imaging (VMI) device[39] coupled to a Wiley−McLaren TOF and is described in detail elsewhere.[40] Briefly, a continuous molecular beam/pyrolysis source (identical to the one described in section II.A except for the nozzle diameter of 50 μm) is used in the SAPHIRS source chamber and skimmed toward the interaction chamber (1 mm diameter). There it crosses perpendicularly the synchrotron beam in the center of the DELICIOUS II spectrometer. After ionization, electrons and ions are extracted from this region by a static field of 666 V/cm. Ions are further accelerated with another static field of 666 V/cm and detected in coincidence with electrons

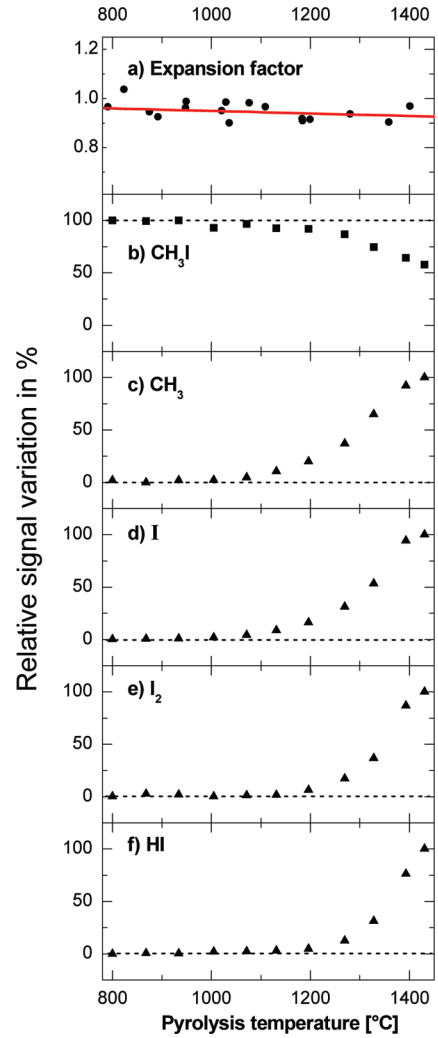

Figure 3. (a) Expansion function calibrated on the normalized NO^+ signal. (b) Signal depletion of the CH_3I precursor in percentage. (c) to (f) Growth percentages of the various observed pyrolysis products as a function of the pyrolysis temperature used in this work. Note that the temperature scale refers to the read temperature on the pyrometer and does not correspond to the gas temperature in the pyrolysis tube at high temperature above 1400 °C (see text).

of any energy between 0 and 6.67 eV, leading to photoelectron photoion-coincidence (PEPICO) spectra.[41,42] The resulting spectra are normalized by the photon flux recorded by a calibrated VUV photodiode (IRD, SXUV100). Note that the same setup has been used in a parallel experiment to study the spectroscopy of the methyl cation and its isotopomers[43] via threshold photoelectron−photoion coincidence spectroscopy (TPEPICO).

To increase the number density of the precursor molecules, the liquid-phase precursors are bubbled into the jet via a helium or argon flow for CH_3I or CH_3NO_2, respectively. Due to its high vapor pressure at ambient temperature, methyl iodide is cooled to −10 °C in the bubbler with a H_2O−NaCl bath. The heating power of the pyrolysis source is adjusted for optimal precursor conversion, i.e., 40 W for nitromethane and 50 W for methyl iodide.

III. Results and Discussion

Ion yield signals for pyrolysis fragments have been recorded at the SOLEIL synchrotron facility over a large VUV range by using both precursors, CH_3I and CH_3NO_2. Absolute cross sections have been measured at a fixed wavelength in laser

experiments (118.2 nm), for the CH_3I precursor only, and have been used to calibrate the cross section curves over the VUV range scanned at the synchrotron facility.

A. Observed Processes for the Pyrolysis of CH_3I. In the temperature range of our pyrolysis source (800−1450 °C), the only observed products in the mass spectra are CH_3, I, HI, and I_2. We therefore assume that two pyrolysis reactions take place

$$CH_3I \xrightarrow{T} CH_3 + I \qquad T \geq T_0 \tag{2}$$

$$CH_3I \xrightarrow{T} CH_2 + HI \qquad T \geq T'_0 \tag{3}$$

where T_0 and T'_0 are the threshold temperatures for pyrolyses 2 and 3, respectively.

Pyrolysis 3 must occur with a much lower probability than pyrolysis 2 and does not necessarily occur at the same temperature. Indeed, this pyrolysis corresponds to the breaking of two bonds accompanied by a concerted elimination leading to the CH_2 radical and HI molecule.

Production of CH_2 and HI could also be interpreted as a reaction consecutive to pyrolysis 2, between the CH_3 and I products. In total, the net balance leading to CH_2 and HI remains the same. Note that no CH_2 signal could be detected in the present experiment, while only the corresponding HI signal was observed. This can be explained by the strong ionization cross section[44] of HI of about 44 Mb as well as a higher mass discrimination factor for HI than for CH_2. Hence, the lack of CH_2 signal seems to be indicative of a small photoionization cross section, as was assumed by Wang et al.[45]

Further reactions also occur, albeit with a lower probability, between products and precursor and between products, since we also observe I_2 as a secondary product. The first reactions to be considered must contain the observed I_2 product and possibly another hydrocarbon product. As said in section II.B.1, the observed mass spectra recorded at the synchrotron radiation from 9 eV up to 15 eV showed no other hydrocarbon species, even those which have a significant photoionization cross section (like, for instance, CH_4 produced by the reaction $CH_3I + HI \rightarrow CH_4 + I_2$). Therefore, under our experimental conditions, the only pertinent reactions yielding I_2 product are

$$CH_3I + I \rightarrow CH_3 + I_2 \tag{4}$$

$$I + I \xrightarrow{M} I_2 \tag{5}$$

Processes 4 and 5 are subsequent reactive steps following the dominant pyrolysis reaction 2. (Note that reaction 4 is equivalent to the combination of reactions 2 and 5.)

A last comment can be added, concerning all other reactions that could occur between products and between products and precursor, leading to hydrocarbon molecules (CH_4, C_2H_6, C_2H_5, C_2H_4, ...) as well as iodo-hydrocarbons (CH_2I, ...). As said above, these reactions have been neglected, thanks to the observed mass spectra recorded with synchrotron radiation. In summary, reactions 2−5 are the only reactions to be considered in the following discussion.

Figure 3b displays the overall decrease of CH_3I signal (corrected by the VUV flux and presented with a percentage scale), and Figure 3c−f displays the increase in product ionization signals from reactions 2 to 5, i.e. of CH_3, I, I_2, and HI, respectively. The data of Figure 3c−f exhibit an apparent saturation effect for the highest temperature point. Indeed, above

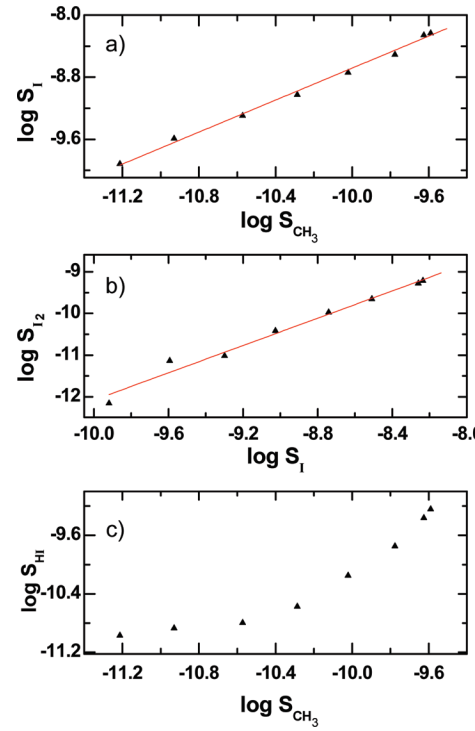

Figure 4. Correlation between various product signals in logarithmic scale: (a) $\log(S_I)/\log(S_{CH_3})$; (b) $\log(S_{I_2})/\log(S_I)$; (c) $\log(S_{HI})/\log(S_{CH_3})$.

1400 °C, the metallic parts of the electrodes may absorb part of the heating power (with a sudden reddish glow), leaving probably the gas inside the tube at a slightly lower temperature than the one measured by the pyrometer, and indicated in the temperature scale of Figure 3. This effect has no implications on the procedure for the absolute cross section measurements described in the following paragraphs, given the negligible effect of the temperature-dependent expansion function for a temperature variation much smaller than 100 °C, as shown in Figure 3.

Figure 4 displays the logarithm of the product signals relative to the logarithm of the CH_3 or I signal, to study the correlation between the various product formations. Only the eight last significant data points, i.e., above the signal noise (see Figure 3), have been considered in this figure. The observed correlation between products shows a linear behavior for $\log(S_I)/\log(S_{CH_3})$ (panel a) and for $\log(S_{I_2})/\log(S_I)$ (panel b) and finally a nonlinear behavior for $\log(S_{HI})/\log(S_{CH_3})$ (panel c). The first two panels (Figures 4a and 4b) illustrate the fact that the CH_3, I, and I_2 fragments result from the same primary pyrolysis, reaction 2. It is worth noting in Figure 4b that the I_2 signal follows the growth of the I signal, according to reactions 4 and 5, but at a slightly higher apparition temperature (see Figure 3d and 3e) than the I signal, as expected for a subsequent reactive channel.

On the other hand, the HI fragment shows a different correlation with the CH_3 signal, as shown by the $\log(S_{HI})/\log(S_{CH_3})$ panel (Figure 4c), indicating that HI is not a secondary product of pyrolysis 2 only but is most probably formed from another reaction, that is, pyrolysis 3.

The threshold temperature T_0 for pyrolysis 2 is approximately 1100 °C as shown by the onsets of CH_3 and I signals in Figures 3b and 3d, while the threshold temperature T'_0 for pyrolysis 3 is slightly higher, about 1200 °C, as shown by the onset of the HI signal in Figure 3f.

Finally, the I_2 and HI signal contributions remain much smaller than the I signal, while their photoionization cross

sections are comparable as will be seen in paragraph D below. This indicates that reactivity as well as the pyrolysis reaction 3 are not so important in our experiment. But, as will be demonstrated below, these small contributions have to be accounted for in the determination of the absolute cross section.

B. Determination of the Absolute Photoionization Cross Section of CH_3I at 118.2 nm. The knowledge of the absolute photoionization cross section of CH_3I at 118.2 nm is necessary for the determination of the absolute photoionization cross section of CH_3 (see paragraph C below). This value has been easily extrapolated from the mass discrimination factor curve of Figure 2. Indeed, a calibrated mixture of CH_3I and propene has been used within the same procedure as described in eq 1 above. This measurement yields the ratio $(F_{CH_3I} \times \sigma_i^{CH_3I})/(F_P \times \sigma_i^P)$. By extrapolating the ratio F_{CH_3I}/F_P of Figure 2 to the mass of CH_3I ($m = 142$ amu), $F_{CH_3I}/F_P = 1.32 \pm 0.17$, we have extracted the following value for the methyl iodide cross section ($\pm 2\sigma$): $\sigma_i^{CH_3I} = (48.2 \pm 7.9)$ Mb at 118.2 nm. It is in very good agreement with the value derived from dipole electron impact techniques[46] for 10.5 eV equivalent photon energy ($\sigma_i^{CH_3I} = 45.7$ Mb). However, it disagrees with the value measured in a previous work on CH_3I photoionization by Arps et al.[47] who found a cross section of 17 Mb within a factor 2. The experimental conditions of Arps et al. measurements are most probably questionable since, in their paper, they published cross section values for standard stable gases far from the well-established values: for instance, they found 9 Mb instead of 2 Mb for NO[27] and 5 Mb instead of 11.2 Mb for acetone.[23] We believe therefore that our value is the first reliable direct determination of the photoionization cross section of CH_3I at 118.2 nm.

C. Procedure for Measuring the Absolute Photoionization Cross Section of CH_3 at 118.2 nm. The procedure for measuring absolute photoionization cross section of CH_3 in the laboratory has been applied only to the case of the CH_3I precursor.

The mass spectra provide ion signals whose peak area is given by the following relationship

$$S_{A^+} \propto I\sigma_i^A[A]F_A \tag{6}$$

where A is a given compound observed in the mass spectrum; I is the intensity of the ionizing photon beam; σ_i^A is the A absolute photoionization cross section; [A] is the A concentration in the beam (corrected by the expansion parameter); and F_A is the A mass discrimination factor evaluated from the calibration curve of Figure 2.

Let us consider two different pyrolysis temperatures T_1 and T_2 with $T_2 > T_1$. According to reactions 2 and 3, the corresponding variation of the concentrations for the CH_3I precursor (depletion) and CH_3 or HI products (growth) is given by

$$\Delta[CH_3I] = \Delta[CH_3] + \Delta[HI] \tag{7}$$

where brackets represent molecular concentrations and the variation of these concentrations with temperature are defined by: $\Delta[CH_3I] = [CH_3I]_{T_1} - [CH_3I]_{T_2}$, $\Delta[CH_3] = [CH_3]_{T_2} - [CH_3]_{T_1}$ and $\Delta[HI] = [HI]_{T_2} - [HI]_{T_1}$.

Combining eqs 6 and 7, one finds the corresponding expression for deriving the photoionization cross section of the methyl radical

$$\sigma_i^{CH_3}{}_{(T_1,T_2)} = \frac{\dfrac{\Delta S_{CH_3^+}}{F_{CH_3}}}{\dfrac{\Delta S_{CH_3I^+}}{F_{CH_3I} \times \sigma_i^{CH_3I}} - \dfrac{\Delta S_{HI^+}}{F_{HI} \times \sigma_i^{HI}}} \tag{8}$$

Since we assume no dependence of the cross sections with temperature, as justified in section E below, all the $\{T_1,T_2\}$ couples should be equivalent to determine the cross section $\sigma_i^{CH_3}$.

Typical signal differences ΔS_{A+} are shown in panel (c) of Figure 1 for two given temperatures.

Statistical estimation of $\sigma_i^{CH_3}$ can be obtained from a sample of $\sigma_i^{CH_3}{}_{(T_1,T_2)}$ data for different $\{T_1,T_2\}$ temperature pairs. To select relevant pairs with ion signal variation beyond the signal-to-noise ratio, only significantly different T_1 and T_2 couples are taken into account. Some of the observables in eq 8 being uncertain (photoionization cross sections, mass discrimination factors, and the expansion function), this procedure is coupled with a Monte Carlo Uncertainty Propagation method.[48] Probability density functions are defined and used to generate N_{MC} random draws for each parameter. Combining these sampled values one-to-one through eq 8 provides a sample of N_{MC} values of $\sigma_i^{CH_3}$ from which statistical estimates are derived. In the present case, N_{MC} is equal to the number of selected $\{T_1,T_2\}$ temperature pairs. The uncertain observables are assumed to have Normal/Gaussian distributions, parametrized by a mean value μ and a standard deviation σ. The following values ($\mu \pm 2\sigma$) have been used:

- photoionization cross section at 118.2 nm: $\sigma_i^{CH_3I} = (48.2 \pm 7.9)$ Mb (see paragraph B above), $\sigma_i^{HI} = (44 \pm 13)$ Mb (see ref 44);

- mass discrimination factors, $F_{CH_3}/F_P = 0.48 \pm 0.09$; $F_{HI}/F_P = 1.31 \pm 0.16$; $F_{CH_3I}/F_P = 1.32 \pm 0.17$ (obtained in the present work, see Figure 2).

Uncertainty on the temperature expansion function is already accounted for in the signal values.

The results are plotted as a histogram in the left panel of Figure 5a. Since the cross section values exhibit an asymmetric distribution on this linear scale, the logarithmic values are also plotted in the right panel of Figure 5a to determine a standard deviation for the log cross section. The latter histogram perfectly fits a Gaussian distribution providing a standard uncertainty which is converted in linear space to an asymmetric 95% confidence interval around the most probable value: $\sigma_i^{CH_3} = 6.7^{+2.4}_{-1.8}$Mb. This asymmetric error bar is indicated by dashed lines on the histogram of the left panel of Figure 5a. This cross-section value is in good agreement, within the error bars, with the absolute measurements at 10.2, 10.460, 10.466, 10.471, and 11 eV, by Taatjes et al.[1]

Note that the effect of neglecting the HI contribution in eq 8 would lead to a smaller value of $\sigma_i^{CH_3}$(5.9 Mb), still within the error bar, meaning that the HI contribution accounts for 10% in the evaluation of the absolute cross section $\sigma_i^{CH_3}$.

Finally, the almost perfect Gaussian shape of the histogram in Figure 5a demonstrates a posteriori that the photoionization cross section $\sigma_i^{CH_3}$ as well as the other cross sections used in eq 8 do not depend on temperature within the experimental conditions explored in this work. The same conclusion is applied to the case of the iodine atom discussed in the next section and Figure 5b.

D. Absolute Measurement of the Photoionization Cross Section of Atomic Iodine at 118.2 nm. Pyrolysis of the CH_3I precursor produces one I atomic fragment for every CH_3 fragment (eq 2). Note that, unlike in the case of the photolysis

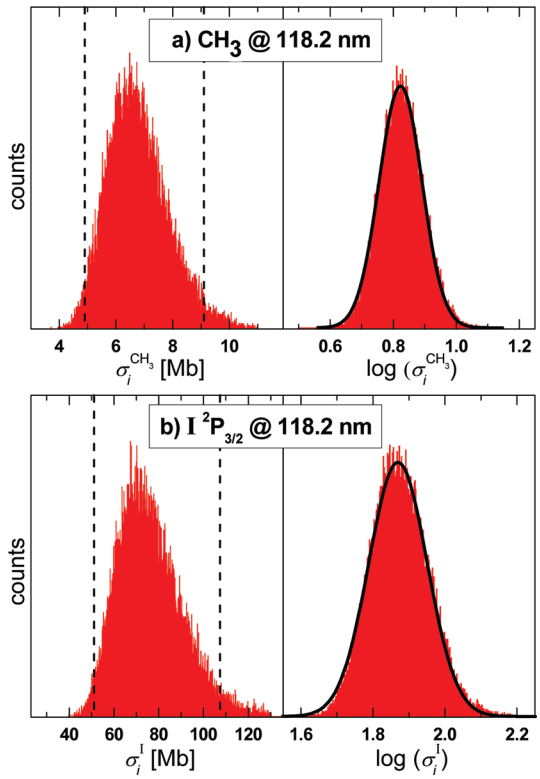

Figure 5. (a) Histogram plots of the linear and logarithmic experimental values measured for CH_3 photoionization cross section at 118.2 nm (red bars) with the best Gaussian fit shown in black line. The full-width at half-maximum (fwhm) of the Gaussian fit gives the (2σ) error bar on the logarithmic value, i.e., 0.136, from which an asymmetric error bar can be extracted for the $\sigma_i^{CH_3}$ value in Mb (the 95% confidence interval is indicated by dashed lines). (b) Histogram plots of the linear and logarithmic measured values for atomic iodine ($^2P_{3/2}$) photoionization cross section at 118.2 nm (red bars) with the best Gaussian fit shown with the black line. The fwhm of the Gaussian fit is 0.161.

process used by Taatjes et al.,[1] in our experiment this fragment is only formed in its $^2P_{3/2}$ ground state as justified in section E below.

A similar procedure as the one described in section C above can be used to determine the iodine absolute photoionization cross section, by adding the I_2 ($\sigma_i^{I_2}$ = (55 ± 16) Mb, ref 49) and HI contributions to the overall iodine production rate and by using the following mass discrimination factors: $F_I/F_P = 1.31 \pm 0.16$ and $F_{I_2}/F_P = 1.36 \pm 0.23$ (see previous paragraph for the other values). The cross section for iodine is then given by

$$\sigma_i^{I} = \frac{\dfrac{\Delta S_{I^+}}{F_I}}{\dfrac{\Delta S_{CH_3I^+}}{F_{CH_3I} \cdot \sigma_i^{CH_3I}} - \dfrac{\Delta S_{HI^+}}{F_{HI} \cdot \sigma_i^{HI}} - 2\dfrac{\Delta S_{I_2^+}}{F_{I_2} \cdot \sigma_i^{I_2}}} \qquad (9)$$

Figure 5b displays the histograms built with the same procedure as for CH_3 in Figure 5a. The right panel displays the logarithmic values well fitted by a Gaussian function and gives rise to the following measured value: $\sigma_i^{I(^2P_{3/2})} = 74^{+33}_{-23}$ Mb. The rather large uncertainty can be traced back to the large uncertainty in cross section values taken from the literature[44,49] and from the extrapolation of the mass discrimination factor (see Figure 2).

E. Absolute Calibration of the Photoionization Yield of CH_3 and I Measured at the Synchrotron Radiation. Figure 6 displays the relative photoionization yield of CH_3 recorded with synchrotron radiation as a function of the photon energy, obtained from the pyrolysis of two precursors CH_3I and CH_3NO_2. We have corrected the photon energy scale on this figure for the effect of the DC extraction field in our detection system on the molecular potential,[50] by shifting the energy scale of the entire spectra by 19 meV (as will be justified in the next paragraph).

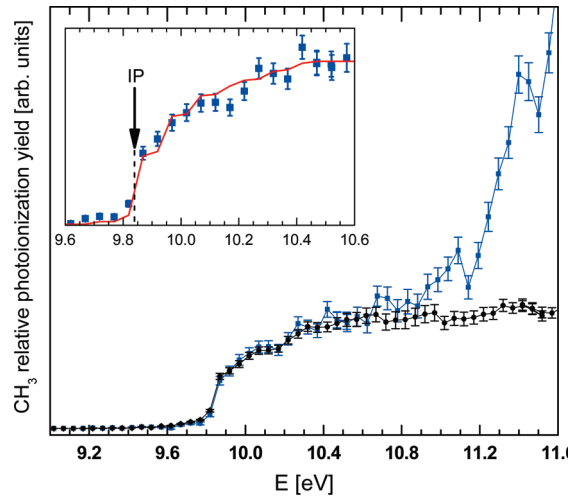

Figure 6. Photoionization yield of CH_3 recorded at the synchrotron radiation as a function of the photon energy, from the pyrolysis of two precursors CH_3I (blue squares) and CH_3NO_2 (black dots). The error bars take into account the counting statistics as well as the VUV photodiode measurement uncertainty. In the inset, the CH_3 experimental data points of the ionization yield from CH_3I precursor are shown together with the corresponding simulation (red line, $T_{vib} = 2100 \pm 500$ K, $T_{rot} = 600$ K, see text). The arrow locates the very accurate IP of ref 57.

In the curve corresponding to the CH_3I precursor (blue squares in Figure 6), the sudden increase of the CH_3 signal around 11 eV can be explained by the onset of the dissociative ionization $CH_3I + h\nu \rightarrow CH_3^+ + I$. Note that the threshold from the literature is set at a higher energy (12.2 eV[51–54]), indicating that in our experiment the CH_3I precursor is still significantly hot in the interaction zone where the molecular beam crosses the synchrotron radiation. A similar onset for dissociative ionization is also observed for the CH_3NO_2 precursor but at higher energies than the observed range of Figure 6. Indeed, the precursor molecules, still present in the molecular beam, might keep a considerable vibrational internal energy (of the order of 9 kT), producing "hot bands" in the photoexcitation process leading to dissociative ionization.

The CH_3 product most probably bears internal vibrational energy following the dissociation via pyrolysis but to a lesser extent than the precursor molecules in the molecular beam. The CH_3 energy population is distributed over vibrational and rotational excited states and may affect the onset of the ionization curve of Figure 6. We have attempted to model the onset of the photoionization curves for the direct ionization of CH_3 produced by pyrolysis of the two precursors, CH_3NO_2 and CH_3I, applying the Franck−Condon (FC) factors found in the literature[55] for excitation of the two active modes in CH_3 ionization,[56] the symmetric stretching mode and the umbrella mode. The model depends on three variables: the adiabatic IP, the vibrational temperature, and the rotational temperature. Since the IP has already been determined very accurately,[57] its value is frozen at 9.839 eV. The rotational temperature has no detectable effect on the present simulation and is fixed at a mean value of 600 K. Only the vibrational temperature is left to vary.

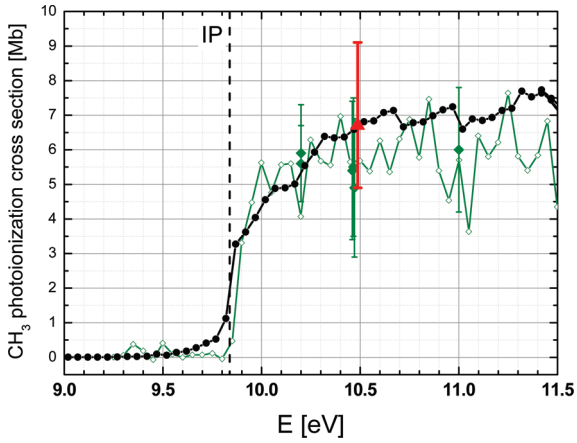

Figure 7. Absolute photoionization cross section of CH_3 measured in this work, from the CH_3NO_2 precursor (black dots, see text). The red triangle with its error bars locates the absolute measurement point used to scale the whole spectrum to an absolute scale. The spectrum obtained by Taatjes et al.[1] is shown for comparison (olive green open diamonds).

The inset of Figure 6 displays in an enlarged scale the simulated onset together with the experimental values in the case of the CH_3I precursor only, for the sake of clarity. For both precursors, there is a satisfactory agreement between the simulated total ion yield and the experiment. The obtained vibrational temperatures for the neutral CH_3 are: (4500 ± 800) K and (2100 ± 500) K for the CH_3NO_2 and CH_3I spectra, respectively. Although these values might seem high, they would only correspond to excitation of one quantum of CH_3 symmetric stretch. Thus, the precursor can easily act as an energy sink and later release this energy into the internal energy of the pyrolysis fragments. It should be noted that the obtained vibrational temperatures depend mainly on the quality of the calculated FC factors from ref 55. Nevertheless, it is worth noting that the vibrational temperature does not affect significantly the ionization yield of CH_3 even at the threshold, as shown by the two curves from both precursors in Figure 6. This was already discussed by Aguirre and Pratt[58] who found that vibrationally excited CH_3 has an almost internal-energy-independent cross section at 118.2 nm for the range of vibrational excitation considered in this work. This point is essential for validating our cross section measurement at 118.2 nm by using a pyrolysis source for radicals.

Note that the simulation presented in the inset of Figure 6 has been performed by neglecting the autoionization processes. The good agreement with the measured signal validates this assumption in the range 9−11.5 eV. It also justifies the fact that the photon energy scale of the entire photoionization spectra, which only involves direct ionization into rovibrational levels of the cation ground state, can be shifted by the same amount to correct for the static field effect of our detection system. The same correction has been applied to our spectrum of Figure 7.

Figure 7 displays the absolute photoionization cross section of CH_3 produced from pyrolysis of CH_3NO_2 calibrated from the 118.2 nm measurement, together with the results of Taatjes et al.[1] for comparison. The two independent measurements of this photoionization cross section are in very good agreement within all the error bars. However, our spectrum exhibits a better signal-to-noise ratio. Note that a difference appears between the curves at the threshold and is not understood at the present time. This difference cannot be ascribed to a temperature effect due to the internal energy of CH_3 in the case of the pyrolysis source, as said above. On the other hand, the shape of the ionization

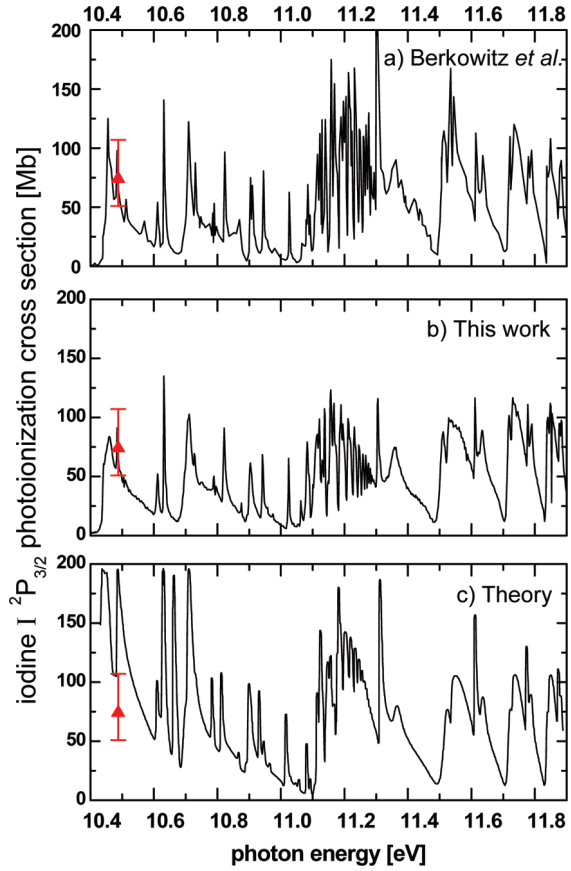

Figure 8. (a) Photoionization cross section of $I(^2P_{3/2})$ recorded as a function of the photon energy between 10.4 and 11.9 eV by Berkowitz et al.[2] and plotted with an absolute scale by using our measured cross section at 118.2 nm. (b) Present data recorded at the synchrotron radiation, from the pyrolysis of CH_3I. (c) Theoretical calculations performed by Robicheaux and Greene.[3] Spectra of (b) and (c) are recalibrated by using the accurately determined absolute photon energy scale of the Berkowitz et al. spectrum of (a).

threshold curve of CH_3 produced by photolysis is not commented on in detail in ref 1. At photon energy higher than 10.5 eV, our cross section curve is on the average about 1 Mb higher than the mean curve of ref 1, but the agreement between ref 1 and our results remains rather satisfactory within all error bars.

Figure 8 displays the absolute photoionization cross section of the iodine atom in its ground state $^2P_{3/2}$, taken from three studies: Figure 8a displays the ionization spectrum obtained by Berkowitz et al. from an AgI evaporation source, at a resolution of 0.28 Å (that is an average photon energy resolution of 3 meV in the observed region).[2] This spectrum has been plotted on an absolute cross section scale by using our measured value $\sigma_i^I = 74$ Mb at 118.2 nm (laser width of about 0.055 nm or 5 meV). Figure 8b displays our ionization spectrum recorded with synchrotron radiation, with a photon energy resolution slightly worse than the Berkowitz et al. spectrum (4 meV) and normalized to an absolute cross section scale by using the same value of σ_i^I at 118.2 nm as above. Figure 8c reports the iodine cross section calculated by Robicheaux and Greene.[3] Note that the spectra of panels (b) and (c) have been wavelength-recalibrated to fit the carefully calibrated photon energy scale of Berkowitz et al.[2] A very good agreement is obtained between the two experimental cross section curves of panel (a) and (b), except for slight discrepancies in amplitude in the region 11.1−11.4 eV. Concerning the overall shape of the spectrum, a fair agreement is also observed between theory and experiment, except for three strong features in the theoretical spectrum

(at 10.44, 10.48, and 10.66 eV) which do not fit properly the experimental data.

IV. Conclusion

The present results show that the combination of synchrotron-based and VUV laser-based experiments using the same radical pyrolysis source provides complementary information critical to the measurement of absolute cross sections. We have measured the cross section of CH_3 between its ionization threshold (at 9.839 eV)[57] and 11.5 eV. The very low effect of vibrational temperature of the CH_3 radical on the cross section curves validates the assumption of a temperature-independent cross section in the range of temperatures used in this work (800−1400 °C). In particular, it validates the procedure for measuring the absolute cross section of CH_3 at 118.2 nm, as was shown by the narrow histograms built from many pyrolysis temperature measurements. During this measurement, calibration of the apparatus function allowed measurement for the first time of the absolute photoionization cross section of CH_3I at 118.2 nm, in good agreement with the value extracted from dipole electron impact measurements.

The atomic iodine I $^2P_{3/2}$ photoionization cross section has been calibrated on an absolute scale for the first time, both on the very high quality ionization curve of Berkowitz et al.[2] and on our measurement.

Special care was taken in this work about the evaluation of the various sources of uncertainties which are generally attached to this kind of absolute measurements. They will improve the confidence given for the implementation of such data in planetary models.

This work presents the first step toward an accurate laboratory study of the photolysis of methane at 121.6 nm related to Titan's atmosphere photochemistry. More generally, accurate measurements of photoionization cross section of such small hydrocarbon radicals are strongly needed for the modeling of the photochemistry of planetary and cometary atmospheres. Similar measurement by using pertinent precursors in our pyrolysis source and the same calibrated experimental setup will be performed in further studies of hydrocarbon and cyano-hydrocarbon radicals.

Acknowledgment. We acknowledge SOLEIL for provision of synchrotron radiation facilities, and we would like to thank the staff of DESIRS beamline for its efficient assistance. We are greatly indebted to Prof. Berkowitz for lending us the original records of the iodine photoionization curves for comparison with our measurements. Financial support from the "Pôle Planétologie" of the PRES UniverSud is acknowledged (contract 2008-53). L.V.M. and B.C.M. are grateful to the CAPES-COFECUB programme for a CAPES fellowship (contract # 525/06).

References and Notes

(1) Taatjes, C. A.; Osborn, D. L.; Selby, T. M.; Meloni, G.; Fan, H.; Pratt, S. T. *J. Phys. Chem. A* **2008**, *112*, 9336.

(2) Berkowitz, J.; Baston, C. H.; Goodman, G. L. *Phys. Rev. A* **1981**, *24*, 149.

(3) Robicheaux, F.; Greene, C. H. *Phys. Rev. A* **1992**, *46*, 3821.

(4) Flasar, F. M.; Achterberg, R. K.; Conrath, B. J.; Gierasch, P. J.; Kunde, V. G.; Nixon, C. A.; Bjoraker, G. L.; Jennings, D. E.; Romani, P. N.; Simon-Miller, A. A.; Bezard, B.; Coustenis, A.; Irwin, P. G. J.; Teanby, N. A.; Brasunas, J.; Pearl, J. C.; Segura, M. E.; Carlson, R. C.; Mamoutkine, A.; Schinder, P. J.; Barucci, A.; Courtin, R.; Fouchet, T.; Gautier, D.; Lellouch, E.; Marten, A.; Prange, R.; Vinatier, S.; Strobel, D. F.; Calcutt, S. B.; Read, P. L.; Taylor, F. W.; Bowles, N.; Samuelson, R. E.; Orton, G. S.; Spilker, L. J.; Owen, T. C.; Spencer, J. R.; Showalter, M. R.; Ferrari, C.; Abbas, M. M.; Raulin, F.; Edgington, S.; Ade, P.; Wishnow, E. H. *Science* **2005**, *308*, 975.

(5) Hébrard, E.; Dobrijevic, M.; Carrasco, N.; Pernot, P.; Bergeat, A.; Hickson, K.; Canosa, A.; Le Picard, S.; Sims, I. R. *J. Phys. Chem. A* **2009**, in press.

(6) Romanzin, C.; Gazeau, M.-C.; Bénilan, Y.; Hébrard, E.; Jolly, A.; Raulin, F.; Boyé-Péronne, S.; Douin, S.; Gauyacq, D. *Adv. Space Res.* **2005**, *36*, 258.

(7) Person, J. C.; Nicole, P. P. *J. Chem. Phys.* **1965**, *43*, 2553.

(8) Person, J. C.; Nicole, P. P. *J. Chem. Phys.* **1968**, *49*, 5421.

(9) Person, J. C.; Nicole, P. P. *J. Chem. Phys.* **1970**, *53*, 1767.

(10) Person, J. C.; Nicole, P. P. *J. Chem. Phys.* **1971**, *55*, 3390.

(11) Rennie, E. E.; Johnson, C. A. F.; Parker, J. E.; Holland, D. M. P.; Shaw, D. A.; Hayes, M. A. *Chem. Phys.* **1998**, *229*, 107.

(12) Robinson, J. C.; Sveum, N. E.; Neumark, D. M. *J. Chem. Phys.* **2003**, *119*, 5311.

(13) Sveum, N. E.; Goncher, S. J.; Neumark, D. M. *Phys. Chem. Chem. Phys.* **2006**, *8*, 592.

(14) FitzPatrick, B. L.; Maienschein-Cline, M.; Butler, L. J.; Lee, S.-H.; Lin, J. J. *J. Phys. Chem. A* **2007**, *111*, 12417.

(15) Kohn, D. W.; Clauberg, H.; Chen, P. *Rev. Sci. Instrum.* **1992**, *63*, 4003.

(16) Chupka, W. A.; Lifshitz, C. *J. Chem. Phys.* **1967**, *48*, 1109.

(17) Schussler, T.; Deyerl, H. J.; Dummler, S.; Fischer, I.; Alcaraz, C.; Elhanine, M. *J. Chem. Phys.* **2003**, *118*, 9077.

(18) Schussler, T.; Roth, W.; Gerber, T.; Alcaraz, C.; Fischer, I. *Phys. Chem. Chem. Phys.* **2005**, *7*, 819.

(19) Flesch, R.; Schürmann, M. C.; Plenge, J.; Hunnekuhl, M.; Meiss, H.; Bischof, M.; Rühl, E. *Phys. Chem. Chem. Phys.* **1999**, *1*, 5423.

(20) Flesch, R.; Plenge, J.; Kühl, S.; Klusmann, M.; Rühl, E. *J. Chem. Phys.* **2002**, *117*, 9663.

(21) Willitsch, S.; Dyke, J. M.; Merkt, F. *Helv. Chim. Acta* **2003**, *86*, 1152.

(22) Hébrard, E.; Dobrijevic, M.; Bénilan, Y.; Raulin, F. *J. Photochem. Photobiol. C: Photochem. Rev.* **2006**, *7*, 211.

(23) Cool, T. A.; Wang, J.; Nakajima, K.; Taatjes, C. A.; McIlroy, A. *Int. J. Mass Spectrom.* **2005**, *247*, 18.

(24) Wang, J.; Yang, B.; Cool, T. A.; Hansen, N.; Kasper, T. *Int. J. Mass Spectrom.* **2008**, *269*, 210.

(25) Carrasco, N.; Dutuit, O.; Thissen, R.; Banaszkiewicz, M.; Pernot, P. *Planetary Space Sci.* **2007**, *55*, 141.

(26) Dobrijevic, M.; Hébrard, E.; Plessis, S.; Carrasco, N.; Pernot, P.; Bruno-Claeys, M. *Adv. Space Res.* **2009**, in press, http://dx.doi.org/10.1016/j.asr.2009.06.005.

(27) Watanabe, K. *J. Chem. Phys.* **1954**, *22*, 1564.

(28) Xia, T. J.; Chien, T. S.; Wu, C. Y. R.; Judge, D. L. *J. Quant. Spectrosc. Radiat. Transfer* **1991**, *45*, 77.

(29) Watanabe, K.; Matsugana, F. M.; Sakai, H. *Appl. Opt.* **1967**, *6*, 391.

(30) Watanabe, K.; Matsugana, F. M.; Sakai, H. *Appl. Opt.* **1967**, *6*, 1220.

(31) Gregory, P. C. *Bayesian logical data analysis for the physical sciences*; Cambridge University Press: Cambridge, UK, 2005.

(32) Sivia, D. S. *Data Anal.: A Bayesian Tutorial*, 1996.

(33) Zhang, T.; Wang, J.; Yuan, T.; Hong, X.; Zhang, L.; Qi, F. *J. Phys. Chem. A* **2008**, *112*, 10487.

(34) Huber, K. P.; Herzberg, G. *Molecular Spectra and Molecular Structure. IV. Constants of Diatomic Molecules*; Van Nostrand Reinhold Co., New York, 1979.

(35) Nahon, L.; Alcaraz, C.; Marlats, J. L.; Lagarde, B.; Polack, F.; Thissen, R.; Lepere, D.; Ito, K. *Rev. Sci. Instrum.* **2001**, *72*, 1320.

(36) Marcouille, O.; Brunelle, P.; Chubar, O.; Marteau, F.; Massal, M.; Nahon, L.; Tavakoli, K.; Veteran, J.; Filhol, J. M. In *Synchrotron Radiation Instrumentation, Pts 1 and 2-AIP Conference Proceedings*; Choi, J. Y., Rah, S. Eds.; American Institute of Physics: New York, 2007; Vol. 879; pp 311.

(37) Mercier, B.; Compin, M.; Prevost, C.; Bellec, G.; Thissen, R.; Dutuit, O.; Nahon, L. *J. Vac. Sci. Technol., A* **2000**, *18*, 2533.

(38) Richard-Viard, M.; Delboulbe, A.; Vervloet, M. *Chem. Phys.* **1996**, *209*, 159.

(39) Garcia, G. A.; Nahon, L.; Harding, C. J.; Mikajlo, E. A.; Powis, I. *Rev. Sci. Instrum.* **2005**, *76*, 053302.

(40) Garcia, G. A.; Soldi-Lose, H.; Nahon, L. *Rev. Sci. Instrum.* **2009**, *80*, 023102.

(41) Baer, T.; Guyon, P.-M. *High Resolution Laser Photoionisation and Photoelectron Studies*; Wiley: New York, 1995.

(42) Baer, T. *Int. J. Mass Spectrom.* **2000**, *200*, 443.

(43) Cunha de Miranda, B. K.; Alcaraz, C.; Elhanine, M.; Noller, B.; Hemberger, P.; Fischer, I.; Garcia, G.; Soldi-Lose, H.; Gans, B.; Vieira Mendes, L. A.; Boyé-Péronne, S.; Douin, S.; Zabka, J.; Botschwina, P. *J. Phys. Chem. A* **2009**, submitted.

(44) Carlson, R. C.; Gerard, P.; Krause, M. O.; Von Wald, G.; Taylor, J. W.; Grimm, F. A. *J. Chem. Phys.* **1986**, *84*, 4755.

(45) Wang, J.-H.; Liu, K.; Min, Z.; Su, H.; Bersohn, R. *J. Chem. Phys.* **2000**, *113*, 4146.
(46) Olney, T. N.; Cooper, G.; Brion, C. E. *Chem. Phys.* **1998**, *322*, 211.
(47) Arps, J. H.; Chen, C. H.; Mccann, M. P.; Datskou, I. *Appl. Spectrosc.* **1989**, *43*, 1211.
(48) BIPM; IEC; IFCC; ISO; IUPAC; IUPAP & OIML. "Evaluation of measurement data - Supplement 1 to the GUM: propagation of distributions using a Monte Carlo method"; ISO/IEC Guide 98-3/Suppl.1:2008, 2008.
(49) Myer, J. A.; Samson, J. A. R. *J. Chem. Phys.* **1970**, *52*, 716.
(50) Merkt, F.; Osterwalder, A.; Seiler, R.; Signorell, R.; Palm, H.; Schmutz, H.; Gunzinger, R. *J. Phys. B: At., Mol. Opt. Phys.* **1998**, *31*, 1705.
(51) Nicholson, A. J. C. Determination of bond dissociation energies from photoionization efficiency curves. In *Recent Developments in Mass Spectrometroscopy*; Hayakawa, K. O. a. T., Ed.; Univ. Park Press: Baltimore, MD, 1970; p 745.
(52) Tsai, B. P.; Baer, T.; Werner, A. S.; Lin, S. F. *J. Phys. Chem.* **1975**, *79*, 570.
(53) Mintz, D. M.; Baer, T. *J. Chem. Phys.* **1976**, *65*, 2407.
(54) Traeger, J. C.; McLoughlin, R. G. *J. Am. Chem. Soc.* **1981**, *103*, 3647.
(55) Botschwina, P.; Flesch, J.; Meyer, W. *Chem. Phys.* **1983**, *74*, 321.
(56) Eppink, A. T. J. B.; Parker, D. H. *J. Chem. Phys.* **1999**, *110*, 832.
(57) Schulenburg, A. M.; Alcaraz, C.; Grassi, G.; Merkt, F. *J. Chem. Phys.* **2006**, *125*, 104310.
(58) Aguirre, F.; Pratt, S. T. *J. Chem. Phys.* **2005**, *122*, 234303.

JP909414D